Random sequential adsorption of spheroidal particles: Kinetics and jamming limit

Zbigniew Adamczyk and Pawel/ Weroński

Citation: The Journal of Chemical Physics **105**, 5562 (1996); doi: 10.1063/1.472409
View online: http://dx.doi.org/10.1063/1.472409
View Table of Contents: http://scitation.aip.org/content/aip/journal/jcp/105/13?ver=pdfcov
Published by the AIP Publishing

Random sequential adsorption of spheroidal particles: Kinetics and jamming limit

Zbigniew Adamczyk[a] and Paweł Weroński
Institute of Catalysis and Surface Chemistry, Polish Academy of Sciences, 30-239 Cracow, ul. Niezapominajek 1, Poland

(Received 14 March 1996; accepted 21 June 1996)

Localized adsorption of hard (noninteracting) spheroidal particles on homogeneous interfaces was analyzed theoretically. In contrast to previous studies concentrated on flat (side on) adsorption in the present approach an unoriented (quasi-three-dimensional) adsorption of prolate and oblate spheroids was considered. By applying the random sequential adsorption (RSA) approach asymptotic analytic expressions were derived for the available surface function (surface blocking parameter) and adsorption kinetics in the limit of low and moderate surface concentrations. The range of validity of the approximate analytical results was determined by numerical simulations of adsorption kinetics performed using the Monte Carlo RSA technique. It was revealed by this comparison that the analytical approximation can be used with a good accuracy for the dimensionless adsorption time τ smaller than two. The numerical calculations also enabled us to determine the maximum (jamming) surface concentrations for unoriented adsorption of spheroids as a function of the elongation or flattening parameter A. It was demonstrated that these jamming concentrations θ_∞ are approached for long adsorption times as $\tau^{-1/4}$, therefore deviating considerably from the Langmuir model used often in the literature. © *1996 American Institute of Physics.* [S0021-9606(96)51536-9]

I. INTRODUCTION

The adsorption of colloid and bioparticles is of large practical significance in various technologies involving filtration steps. Learning about the mechanisms and kinetics of these phenomena is also relevant for polymer and colloid science, biophysics, and medicine, enabling a better control of protein and cell separation processes, enzyme immobilization, thrombosis, biofouling of transplants and artificial organs, etc.

It is known that the shape of surfactant molecules and bioparticles deviates significantly from perfect spheres analyzed usually in various theoretical and experimental studies of adsorption kinetics. Thus, for example, the blood platelets can be treated as oblate spheroids (disks) having a rather irregular cross-section area. On the other hand the shape of important globular proteins like bovine serum albumin (BSA)[1] or fibrinogen[2–4] resembles prolate spheroids with the axis ratio about 3.5 and 5–7, respectively. The same concerns E. Coli bacteria having the shape of a prolate spheroid with the axis ratio of about two.[5]

Other examples of highly anisotropic particles (usually of platelet form) are the clay mineral, e.g., kaolinite and montmoryllonite, pigments, and synthetic inorganic colloids: gold, silver iodize, silver bromide, barium sulfate, hafnium oxide, etc.[6–8] Also, model polymeric colloid systems of nonspherical monodisperse particles (e.g., Teflon™ or polystyrene latexes) often occur in practice.[9]

It has been experimentally observed[10–12] that adsorption of bioparticles and colloids is essentially irreversible and localized due to attractive dispersion and electrostatic interactions with the interface. The accumulation of particles at interfaces due to these interactions is of a limited extent, however, due to the occurrence of the volume excluded effects (also called surface blocking effects). Thus, both the kinetics of particle adsorption and the maximum surface concentration (jamming concentration) are influenced by the magnitude of the particle–particle repulsive interaction. In some cases, e.g., for concentrate electrolytes, the extent of these interactions can be effectively reduced to values which are negligible in comparison with particle dimensions. Then, the adsorbing particles can be treated as interacting via the hard particle potential and their adsorption can be described in terms of simple models, the most widespread being the random sequential adsorption (RSA) approach.[13–18] The basic assumptions of the model are as follows:

(i) Particles are placed at random on a target (interface) of an isotropic character, i.e., every position on the target is statistically equivalent.
(ii) If the adsorbing particle overlaps with any preadsorbed particles it disappears with unit probability.
(iii) Otherwise the particle is assumed adsorbed at a given point over the target; once the particle is adsorbed its position (and orientation) is permanently fixed (localized, irreversible adsorption).
(iv) The process is continued until the entire surface is completely covered and no more particles can be accommodated, thus the ''jamming'' or maximum parking limit is attained characterized by the surface concentration θ_∞.

Despite the simplicity of the underlying assumptions the

[a]Author to whom all correspondence should be addressed. Electronic mail: ncadamcz@cyf-kr.edu.pl

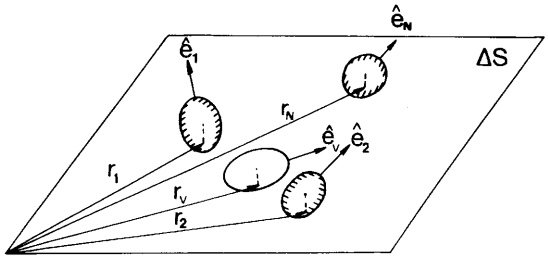

FIG. 1. A schematic representation of the 3D random sequential adsorption of spheroidal particles on a planar interface.

topology of particle distributions generated in RSA processes becomes complex for higher surface concentrations and cannot be analyzed in terms of the well-founded Markoff chain theory. As a consequence of the perfect ''memory'' of the RSA sequences, no exact analytical description valid for the entire range of surface concentrations has been formulated yet except for the one-dimensional case (adsorption on a line).[18]

For the two-dimensional (2D) adsorption, discrete lattice models were often used[17] enabling one to derive series expansions for adsorption kinetics and the available surface function (ASF).

On the other hand, Tarjus *et al.*[16] formulated a systematic description of continuous RSA processes of arbitrary dimensionality using the distribution function approach. This allowed them to derive a Kirkwood–Salsburg-type hierarchy for the ASF functions which was then solved in terms of diagramatic expansions valid for low and moderate concentrations. The formalism is supposed to be valid for anisotropic particles as well, although no explicit results were given.

A complete description of a continuous RSA process in two and three dimensions (3D) was achieved by using Monte Carlo type computer simulations. In this way both the adsorption kinetic (determined by the available surface function ϕ) and the maximum concentration (2D and 3D) for hard[13–15,19] and interacting[12,20,21] spherical particles have been numerically determined.

On the other hand, the RSA results for nonspherical particles are rather scarce and concern exclusively the two-dimensional (2D) cases, i.e., particles were assumed to adsorb with the symmetry axis oriented parallel to the interface (side-on adsorption). In this way adsorption of cubes (more precisely squares) and cylinders (rectangles) was considered in Refs. 22, 23, and 24, respectively. Talbot *et al.*[25] analyzed systematically in terms of the RSA method both the kinetics and maximum jamming concentrations of spheroids (ellipses) of various aspect ratios ranging from 0.8 to 0.2. The jamming limit, the high and low coverage asymptotic adsorption behavior of cylinders, spheroids, and spherocylinders was also determined in precise RSA simulations performed in Refs. 26 and 27.

The 2D adsorption of spheroidal particles interacting via the screened electrostatic interactions was recently studied in Refs. 28 and 29.

To our knowledge, no numerical results were reported in the literature for the important case where anisotropic particles can undergo adsorption not only side on but also under arbitrary orientation of the symmetry axis relative to the interface. This adsorption regime, referred to for sake of convenience as the three-dimensional (3D) regime, seems pertinent to surfactant and protein adsorption when the rotation of the molecules becomes inhibited upon contact with the interface due to, e.g., electrostatic interactions.

Thus, the main goal of our paper is to fill this gap by developing the RSA model for the 3D adsorption of spheroidal particles, either of prolate (elongated) or oblate (flattened) shape. Both the adsorption kinetics and the maximum jamming concentrations shall be determined in relation to particle geometry. Also analytical expressions in the form of the low density expansion are formulated. Preliminary results obtained for elongated spheroids have been presented in our previous work.[30]

II. THE LOW DENSITY EXPANSION

Let us consider the random sequential adsorption (RSA) of hard spheroidal particles at a homogeneous interface whose surface area ΔS for the sake of convenience is normalized to unity (cf. Fig. 1). The basic assumptions of our model are as follows.

(i) Each particle can adsorb under arbitrary orientation which is uniquely defined by the orientation vector $\hat{\mathbf{e}}$ (see Fig. 1); for prolate spheroids $\hat{\mathbf{e}}$ is directed parallel to the longer axis $2a$ and for oblate spheroids parallel to the shorter axis $2b$.

(ii) Adsorbed particles form a rigid, physical contact with the interface, i.e., the surface to surface distances equal zero and their orientations and contact positions become time independent (localization postulate).

(iii) The interface is microscopically homogeneous which means that adsorption probability density has a constant and continuous value over the entire interface.

Let the RSA process proceed for some time so there are N particles adsorbed at the interface under arbitrary positions (characterized by the surface position vectors measured relative to a space fixed coordinate system $\mathbf{r}_1, \mathbf{r}_2,...,\mathbf{r}_N$) and orientations, characterized by the vectors $\hat{\mathbf{e}}_1, \hat{\mathbf{e}}_2,...,\hat{\mathbf{e}}_N$, (cf. Fig. 1). The probability p_v of adsorbing an additional $N+1$ particle (referred to as the virtual particle) having the orientation $\hat{\mathbf{e}}_v$ somewhere at the interface is then given by

$$p_v = S_{\mathrm{av}}/\Delta S = 1 - S_{\mathrm{ex}}/\Delta S = 1 - S_{\mathrm{ex}}, \tag{1}$$

where S_{av} is the available (unblocked) surface area over the interface where the virtual particle center can be located and S_{ex} is the excluded (blocked) area.

Obviously, the probability p_v defined by Eq. (1) depends not only on $\hat{\mathbf{e}}_v$ but also on the size of the particle relative to the size of the adsorption plane and positions and orientations of all N preadsorbed particles. In principle p_v can be calculated for a given system from the double integral:

$$p_v = \int Hv(h_m)\, d\mathbf{r}_v , \tag{2}$$

where Hv is the Heaviside unit step function and h_m is the minimum surface to surface distance between particles.

In order to get rid of the troublesome dependence of p_v on the size of the system and the boundary conditions at the edges of the simulation plane, one has to consider large particle populations or take ensemble averages from many smaller sized surface elements. In this limit the averaged probability $\overline{p_v}$ can be identified with the available surface function ϕ[3], i.e.,

$$\phi(\hat{\mathbf{e}}_v, N) = \overline{p_v} .$$

An explicit analytical calculation of ϕ by evaluating the double integrals as defined by Eq. (2) is not feasible because the statistical properties of the RSA processes are not known *a priori*. Exact calculation of ϕ can only be performed numerically using the Monte Carlo simulation technique as discussed later on.

However, useful approximations can be derived in the limit of low surface concentrations when exploiting the results of Schaaf and Talbot,[15] who showed that for hard spherical particles (of radius a) the ASF can be expressed in the form

$$\phi(N) = 1 - S_1 + S_2 - S_3 + \cdots \tag{3}$$

with

$$S_n = \frac{1}{n!} \int \int \cdots \int A_n(\mathbf{r}_1, \ldots, \mathbf{r}_n) \times \rho^{(n)}(\mathbf{r}_1, \ldots, \mathbf{r}_n, N)\, d\mathbf{r}_1, \ldots, d\mathbf{r}_n ,$$

where A_n are the common (overlapping) areas of the exclusion circles (drawn around each adsorbed particle by rotating the virtual particle by the angle 2π), $A_1 = 4\pi a^2$ is equal to the area excluded by a single particle, and $\rho^{(n)} = N^n g^{(n)}$ are the n-particle generic distribution functions ($g^{(n)}$ are the n-particle distribution functions).

For spheroidal particles ϕ is dependent not only on N but also on the orientation vector $\hat{\mathbf{e}}_v$, i.e.,

$$\phi(\hat{\mathbf{e}}_v, N) = 1 - S_1(\hat{\mathbf{e}}_v, N) + S_2(\hat{\mathbf{e}}_v, N) - S_3(\hat{\mathbf{e}}_v, N) + \cdots , \tag{4}$$

with S_n to be calculated from the multiple integrals over positions and orientations

$$S_n(\hat{\mathbf{e}}_v, N) = \frac{1}{n!} \int \int \cdots \int A_n(\mathbf{r}_1, \ldots, \mathbf{r}_n, \hat{\mathbf{e}}_1, \ldots, \hat{\mathbf{e}}_n, \hat{\mathbf{e}}_v) \times \rho^{(n)}(\mathbf{r}_1, \ldots, \mathbf{r}_n, \hat{\mathbf{e}}_1, \ldots, \hat{\mathbf{e}}_n, N)\, d\mathbf{r}_1 \ldots d\mathbf{r}_n (d\hat{\mathbf{e}}_1/2\pi) \ldots (d\hat{\mathbf{e}}_n/2\pi) \tag{5}$$

$$= \theta^n \frac{1}{S_g^n n!} \int \int \cdots \int A_n g^{(n)} d\mathbf{r}_1 \ldots d\mathbf{r}_n \times (d\hat{\mathbf{e}}_1/2\pi), \ldots, (d\hat{\mathbf{e}}_n/2\pi),$$

where $\theta = N S_g$ is the dimensionless surface concentration of adsorbed particles and S_g is the scaling area, e.g., one of the geometrical cross sections of a spheroid.

As mentioned, Tarjus *et al.*[16] presented a more general approach aimed at expressing ϕ (and analogous functions for multiplets) in terms of power series expansion of θ. The coefficient of this expansion can be calculated from Mayer diagrams similar to the virial coefficients. However, the Mayer functions and the correlation functions for spheroidal particles are difficult to express explicitly in terms of particle center to center distances and particle orientations.[31] Moreover, for elongated objects there appear to be problems with the cancellation of various diagrams.[32] Therefore, we think that the approach adopted above based on calculating exclusion and overlapping areas for various particle configurations is more convenient for this particular problem.

Knowing the available surface function ϕ for a given orientation of the virtual particle one can describe the kinetics of irreversible adsorption of spheroids by generalizing the integral equation given by Viot *et al.*[26]

$$\frac{dN}{dt} = \int k_a(\hat{\mathbf{e}}_v) g_v^{(1)}(\hat{\mathbf{e}}_v)\, \phi(\hat{\mathbf{e}}_v, N)(d\hat{\mathbf{e}}_v/2\pi), \tag{6}$$

where k_a is the adsorption rate constant (the transfer rate of a particle for a given orientation from the bulk to the interface[12]) and $g_v^{(1)}$ is the orientational distribution function of the adsorbing particle.

An explicit formulation of Eq. (6) in the general case seems rather cumbersome. However, for many practical situations one can assume with a good accuracy that both the adsorption rate constant k_a and $g_v^{(1)}$ are independent of the orientation vector $\hat{\mathbf{e}}_v$ (as is the case, for example, in the absence of external force field orienting particles). Under such circumstances Eq. (6) simplifies to the form used previously[14,15,26,27]

$$\frac{dN}{dt} = k_a \overline{\phi}(N), \tag{7}$$

where $\overline{\phi}(N) = \int \phi(\hat{\mathbf{e}}_v, N)\ (d\hat{\mathbf{e}}_v/2\pi)$ is the orientation averaged ASF.

Moreover, in the limit of low densities, assuming a quasirandom distribution of particles,[16,27] one can formulate Eq. (7) by using the expression for ϕ, Eq. (5) in the concise dimensionless form

$$\frac{d\theta}{d\tau} = 1 - C_1\theta + C_2\theta^2 + 0(\theta)^3 . \tag{8}$$

$\tau = S_g k_a\, t$ is the dimensionless adsorption time and C_1 and C_2 are the dimensionless constants (independent of θ and the orientation angles) given by

$$C_1 = \langle A_1 \rangle / S_g , \qquad C_2 = \frac{\langle A_2 \rangle}{2S_g} , \tag{9}$$

where

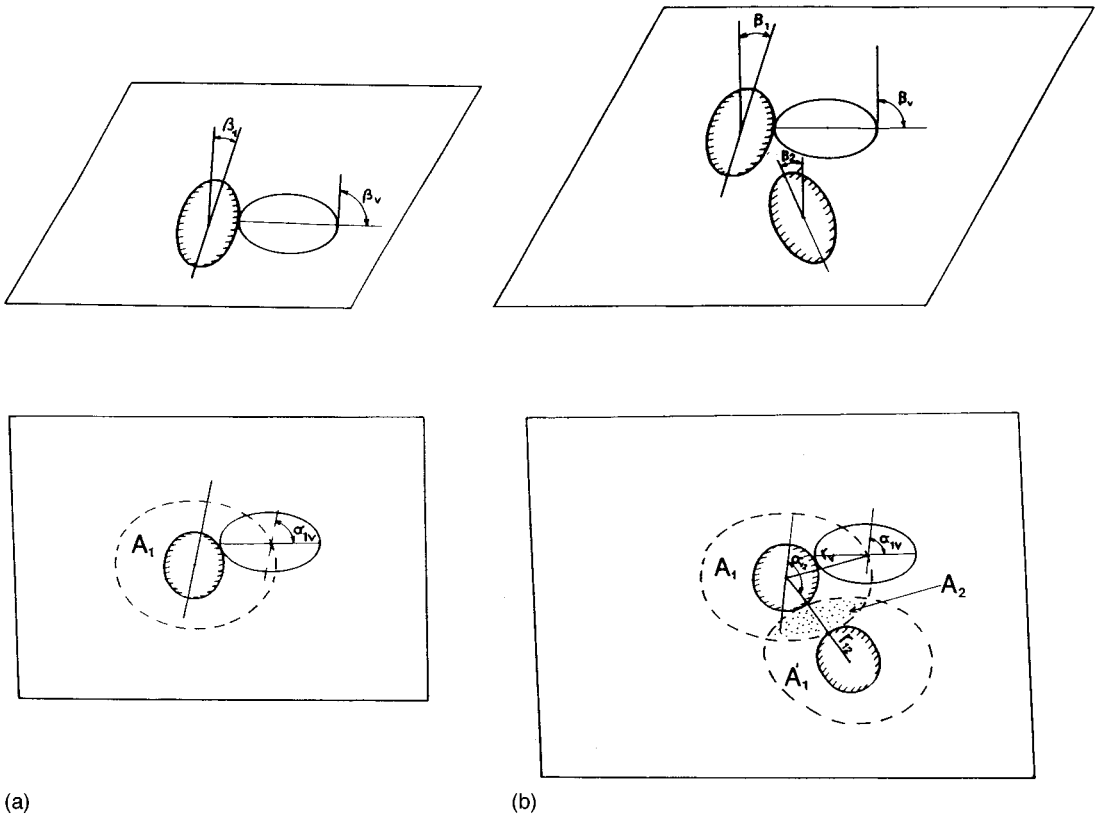

FIG. 2. (a) The excluded area A_1 for the two spheroid configuration: one adsorbed (shadowed) and adsorbing (virtual) depending on the orientation angles β_1, β_v, and α_{1v}. (b) The excluded areas A_1 and A_1' and the overlapping area $A_2 = A_1 \cap A_1'$ for the three-spheroid configuration: two adsorbed (shadowed) and one adsorbing (virtual).

$$\langle A_1\rangle = \frac{2}{\pi^3}\int_0^{2\pi} d\alpha_{1v}\int_0^{\pi/2} d\beta_1\int_0^{\pi/2} A_1(\alpha_{1v},\beta_1,\beta_v)d\beta_v,$$

$$\langle A_2\rangle = \frac{2}{S_g\pi^5}\int_0^{2\pi} d\alpha_{12}\int_0^{2\pi} d\alpha_{1v}\int_0^{\pi/2} d\beta_1\int_0^{\pi/2} d\beta_2 \times\int_0^{\pi/2} d\beta_v\int A_2(\alpha_{12},\alpha_{1v},\beta_1,\beta_2,\beta_v,\mathbf{r}_{12})d\mathbf{r}_{12}$$

are the averaged excluded and overlapping areas, respectively, and $\mathbf{r}_{12}=\mathbf{r}_1-\mathbf{r}_2$ is the center to center vector of the particle pair (the remaining coordinates occurring in this equation are defined in Fig. 2).

The excluded area A_1 can be calculated from the surface integral

$$A_1 = \int [H(h_m)-1]d\mathbf{r}_v, \tag{10}$$

and $A_2 = A_1 \cap A_1'$ is the common (overlapping) area [see Fig. 2(b)].

Considering this definition one can deduce by performing a dimensional analysis that the $A_2\, d\mathbf{r}_{12}$ integral occurring in Eq. (9) should be of the order of $A_1^2 \sim \langle A_1\rangle^2$. Consequently the ratio C_1^2/C_2 should be constant.

Moreover, as shown by Tarjus *et al.*[16] and Ricci *et al.*[27] the above defined constants C_1 and C_2 characterizing the RSA process are identical to equilibrium adsorption systems and are, therefore, connected with the second B_2 and the third virial coefficients B_3 through the dependencies

$$\begin{aligned} C_1 &= 2B_2, \\ C_2 &= 2B_2^2 - \tfrac{3}{2}B_3 = qC_1^2, \end{aligned} \tag{11}$$

where

$$q = \frac{1}{4}\left(2 - \frac{3}{2}\frac{B_3}{B_2^2}\right)$$

is the dimensionless constant.

We have retained only the three terms of the series expansion Eq. (8) for two reasons.

(i) Inclusion of higher terms leads to complicated integrals of high dimensionality whose evaluation becomes more involved than direct Monte Carlo calculations of ϕ.

(ii) A simple analytical equation for adsorption kinetics can be derived when considering the three terms only.

It seems that the integrals occurring in Eq. (9) cannot be evaluated analytically except for the case of spheres, when $\langle A_1\rangle = 4\pi a^2$, $\langle A_2\rangle = 12\sqrt{3}a^2$, which gives for C_1 and C_2 the simple expressions (when using $S_g=\pi a^2$ as the scaling variable)

$$C_1 = 4,$$

$$C_2 = \frac{6\sqrt{3}}{\pi}.$$

Similarly, for the flat orientation of spheroids one can express $\langle A_1 \rangle$ analytically as[32,33]

$$\langle A_1 \rangle = 2\pi ab + \frac{P^2}{2\pi}, \tag{12}$$

where P is the perimeter of the ellipse given by the complete elliptic integral of the second kind. In the limit when $b/a = A \to 0$ (needlelike objects) one can deduce that $\langle A_1 \rangle \to 8a^2/\pi$.[32] Then, using πab as the scaling variable S_g one can show that the C_1 constant for ellipses diverges according to $8/(\pi^2 A)$. As a consequence of Eq. (11), C_2 diverges also as $q\ 64/(\pi^4 A^2)$. The q constant was determined by Tarjus *et al.*[32] to be 0.307 by performing tedious analytical integrations.

It seems that for 3D adsorption of spheroids any analytical solutions are difficult to find even in the limiting case when $A \to 0$. It can be easily estimated, however, by considering various configurations of two prolate spheroids that in this limit $\langle A_1 \rangle \sim \pi ab$ (e.g., for one spheroid lying side on and the other oriented perpendicular to the adsorption plane $A_1 \to \pi ab$, for $A \to 0$). Unlike the 2D case, $\langle A_1 \rangle$ is supposed to depend not only on the length of the objects but on its geometrical shape and should, therefore, be different for thin cylinders or spherocylinders.

Choosing again $S_g = \pi ab$ as the scaling variable one can estimate that for the 3D case C_1 approaches a constant value of the order of unity in the limit of very thin objects.

On the other hand, for oblate spheroids one can estimate that $\langle A_1 \rangle \sim a^2$, which suggests that using $S_g = \pi a^2$ as the scaling variable one should obtain a constant value of C_1 in the limit of $A \to 0$ (thin disks).

In general the multiple integrals occurring in Eq. (9) can only be evaluated numerically. In order to calculate C_1 one has to evaluate fivefold definite integrals and for C_2 ninefold integrals. Due to the high dimensionality of these integrals the usual numerical integration schemes (e.g., the generalized Simpson method) are totally inefficient, especially for smaller values of A. Therefore, we calculated these multiple integrals by applying the standard Monte Carlo method[34] which is based on the relationship

$$\int_{\Delta V} \Omega dV = \langle \Omega \rangle \Delta V, \tag{13}$$

where ΔV is the space element (of arbitrary dimension) for which the multiple integral should be evaluated and

$$\langle \Omega \rangle = \frac{1}{N_t} \sum \Omega_n$$

is the averaged value of the function Ω within the space element ΔV determined from N_t trials generated at random with uniform probability.

The results of numerical calculations of the C_1 constant performed according to the above Monte Carlo integration method for prolate spheroids characterized by various elongations are plotted in Fig. 3. In order to facilitate the comparison of the our 3D results with the well-studied case of the 2D (flat) adsorption we have chosen $S_g = \pi ab$, i.e., the

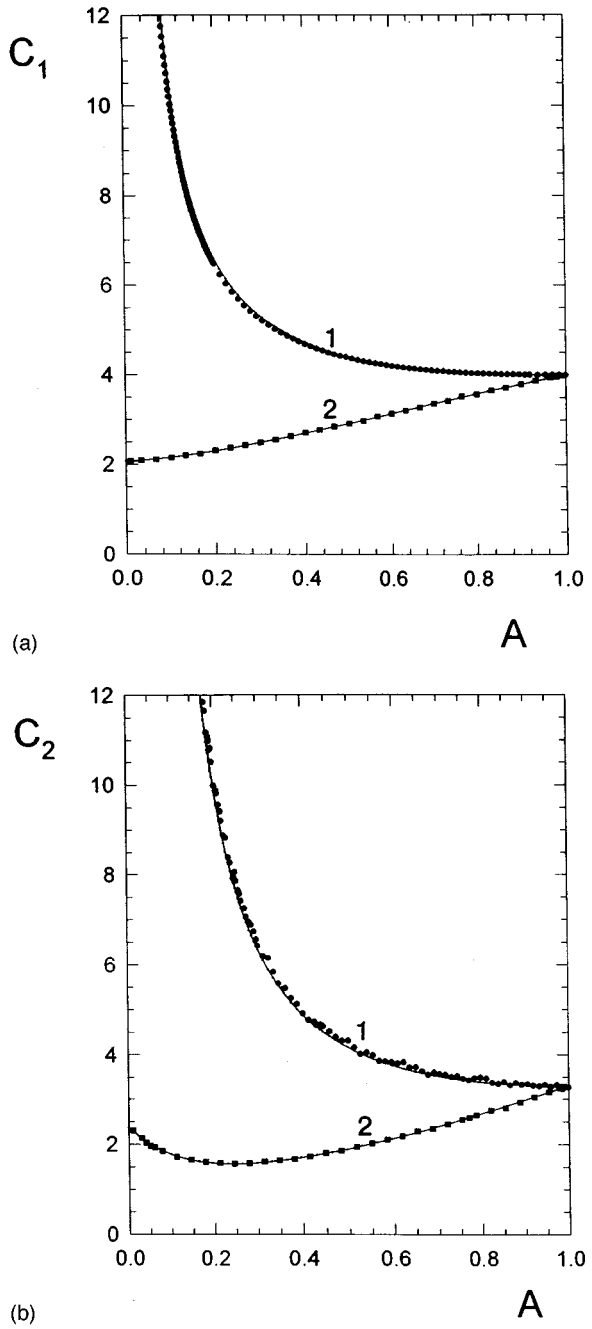

FIG. 3. (a) The dependence of the C_1 constant on the $A = b/a$ parameter determined by the MC-RSA simulations (points) for prolate spheroids: (1) 2D adsorption (flat orientation); (2) 3D adsorption. The continuous line denotes the values derived from the interpolating functions given by Eqs. (14) and (15). (b) The dependence of the C_2 constant on the A parameter determined by the MC-RSA simulations (points) for prolate spheroids: (1) 2D adsorption; (2) 3D adsorption. The continuous line denotes the values derived from the interpolating functions given by Eq. (15) (3D adsorption) and in Ref. 29 (2D adsorption).

surface area of the major ellipse as discussed previously. As can be seen in Fig. 3, in contrast to the 2D case for the 3D adsorption the value of C_1 decreased monotonically with A attaining 2.08 for $A=0.01$ (the lowest value of this parameter used in our calculations).

It was found that the simplest polynomial which reflected well our simulation data had the form

$$C_1=2.07+0.811A+2.37A^2-1.25A^3. \tag{14}$$

As can be deduced, for $A=1$ this expressions matches the limiting value for spheres equal to 4 and for $A\to 0$ approaches the constant value of 2.07, in accordance with the estimation presented above. This value can, therefore, be treated as the extrapolated jamming limit for spheroidal needles.

By comparison, for the 2D adsorption C_1 was described by the approximate formula[29]

$$C_1=\frac{4(\pi^2-4)}{\pi^2}+\frac{8}{\pi^2}\left(A+\frac{1}{A}\right). \tag{15}$$

In this case C_1 diverges in the limit of very elongated spheroids as $8/(\pi^2 A)$. Note that for cylinders $C_1\to 2/(\pi A)$ in this limit.

This prediction has practical significance, indicating that under 3D adsorption conditions the surface blocking effects are much less pronounced for elongated objects in comparison with the flat adsorption.

The dependence of the C_2 constant on the A parameter calculated numerically by the Monte Carlo integration of Eq. (9) is plotted in Fig. 3(b). The continuous line in Fig. 3(b) represents the results calculated from the fitting function given by

$$C_2=\frac{3.88A^2-0.301A+0.670}{A+0.283}. \tag{16}$$

Again, the limiting value for spheres equal to $6\sqrt{3}/\pi=3.31$ is matched whereas for $A=0$, C_2 approaches the constant value of 2.36.

Analogous calculations performed for the oblate spheroids are shown in Figs. 4(a) and 4(b). In order to relate the 3D results to flat adsorption we have assumed $S_g=\pi a^2$, i.e., the surface area of the major circle. As can be seen in Fig. 4(a) for the oblate spheroids the $C_1=2B_2$ constant decreases monotonically with decreasing A and attains for $A=0.0001$ (the lowest limit of our simulations) a value of 1.60, i.e., slightly smaller than for the prolate spheroids. It has been found that C_1 for oblate spheroids can be well approximated by the simple polynomial of A,

$$C_1=1.59+2.80A-0.388A^2. \tag{17}$$

A similar monotonic decrease in the C_2 constant with decreasing A was predicted from the Monte Carlo (MC) calculations as shown in Fig. 4(b). Thus, the C_2 vs A dependence exhibits no minimum in contrast to the prolate spheroid case. The interpolating function for C_2 was found to be

$$C_2=0.700+1.83A+0.776A^2. \tag{18}$$

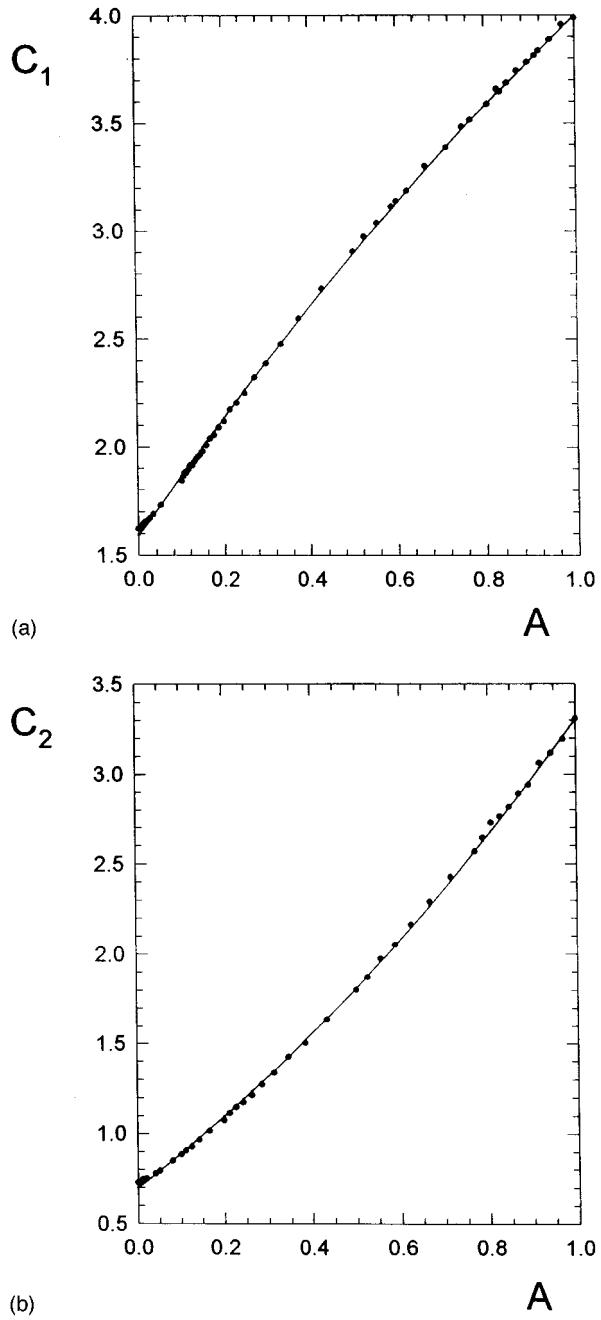

FIG. 4. (a) The dependence of the C_1 constant on A determined by the MC-RSA simulations (points) for oblate spheroids. The continuous line denotes the values derived from the interpolating function given by Eq. (17). (b) The dependence of the C_2 constant on the A parameter determined by the MC-RSA simulations (points) for oblate spheroids. The continuous line denotes the values derived from the interpolating function given by Eq. (18).

Knowing the constants C_1 and C_2 one can integrate Eq. (8) analytically obtaining the explicit kinetic equation connecting the dimensionless surface concentration with the dimensionless adsorption time τ. When $4C_2/C_1^2<1$ the solution becomes

$$\theta(\tau)=\theta_1\frac{1-\exp(-pC_1\tau)}{1-\frac{\theta_1}{\theta_2}\exp(-pC_1\tau)}, \tag{19}$$

where

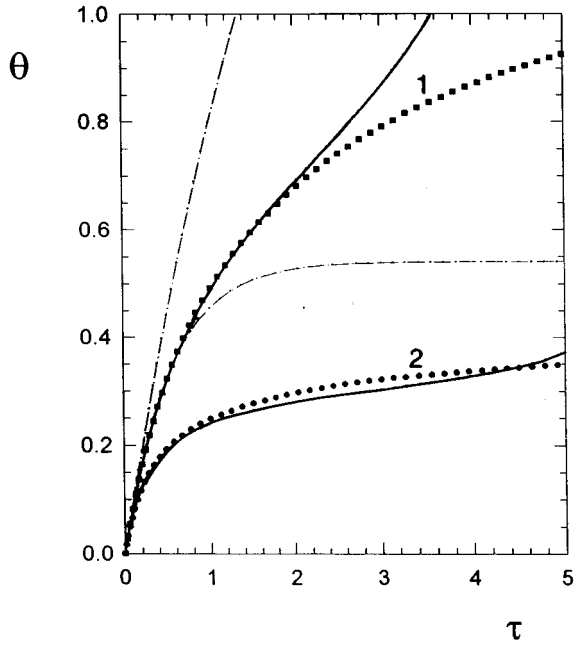

FIG. 5. Kinetics of prolate spheroid adsorption. The dependence of the dimensionless concentration $\theta=\pi abN$ on the dimensionless adsorption time τ determined numerically (points) for $A=0.2$: (1) 3D adsorption; (2) 2D adsorption. The continuous line denotes the analytical results calculated from Eqs. (19) and (20). The -·- lines denote the results stemming from the Langmuir model, Eq. (21).

$$\theta_1=\frac{C_1}{2C_2}[1-p],$$

$$\theta_2=\frac{C_1}{2C_2}[1+p],$$

$$p=\left(1-\frac{4C_2}{C_1^2}\right)^{1/2}.$$

On the other hand, if $4C_2/C_1^2>1$ and

$$p=\left(\frac{4C_2}{C_1^2}-1\right)^{1/2},$$

the solution assumes the form

$$\theta(\tau)=\frac{2}{C_1p}\frac{\tan\frac{1}{2}C_1p\tau}{\left[1+\frac{1}{p}\tan\left(\frac{1}{2}C_1p\tau\right)\right]}. \tag{20}$$

It should be mentioned that using the Langmuir model with the ASF given by $1-\theta/\theta_L$ (where θ_L is the empirical ''monolayer'' concentration) one can derive the following kinetic equation:

$$\theta(\tau)=\theta_L(1-e^{-1/\theta_L\tau}). \tag{21}$$

Equations (19) and (20) are supposed to accurately describe the adsorption kinetics of spheroidal particles in 3D in the limit of low and moderate surface concentrations.

It should be noted that these equations are applicable for equilibrium adsorption as well since they were derived using the first three terms of the ASF expansion which are identical for RSA and equilibrium situations.[16]

However, an exact estimation of the range of validity of Eqs. (19) and (20) can only be achieved in terms of the MC-RSA simulations as described in Sec. III.

III. RESULTS OF NUMERICAL SIMULATIONS

The MC-RSA simulation algorithm. The algorithm of the RSA simulations of 3D adsorption of spheroids was analogous to that described previously for the 2D case[12,28,29] and consisted of the two main calculation modules repeated in a loop.

(i) The virtual (adsorbing) particle was created having the surface coordinates (x_v,y_v) and the orientation α_v, β_v relative to a space-fixed coordinate system (the z_v coordinate of the virtual particle was determined by the β_v orientation angle via the dependence $z=\sqrt{a^2\cos^2\beta_v+b^2\sin^2\beta_v}$). This was achieved using a high-quality pseudorandom number generator giving a uniform distribution of random numbers within the range 0–1 with minimum sequential correlations. The size of the square simulation plane ΔS was normalized to unity and the relative surface area of the virtual particle S_g with respect to ΔS was usually 2×10^{-4}. At the perimeter of the simulation plane the periodic boundary conditions were applied.[29]

(ii) Then, the overlapping test was performed by applying the Vieillard–Baron overlap criteria for spheroids in space;[35] if the virtual particle did not overlap with any previously adsorbed particle then it was taken as adsorbed at the point (x_v,y_v) with the orientation α_v,β_v (these coordinates were stored and the number of adsorbed particles N was increased by one). If overlapping occurred then the simulation step was repeated and the number of simulation attempts N_{att} was increased by one.

The simulation scheme was repeated until no more particles could be adsorbed and the limiting (jamming) particle concentration θ_∞ was attained. This requires, however, excessively long simulation times so we found it considerably more efficient to calculate θ from a linear extrapolation of the long time value of θ as discussed later on. Usually, for a typical value of $A=0.2$, about 10^9 simulation attempts were required for achieving a satisfactory accuracy of determining θ_∞.

It should be noted that for concentrations close to jamming and for lower A values some of the available targets may possess a form resembling ''bottles.'' This means that in order to fill these targets as assumed in our model, there must appear a physical mechanism responsible for the change of particle orientation. This can be, e.g., the rotary Brownian motion occurring universally under all practical situations. Thus, in this respect, our model seems to come

closer to reality than those based on the straight line trajectories approach.

Since the RSA simulations are very time consuming (especially at higher surface concentrations and for elongated particles) optimization of the overlapping test (which is repeated billions of times for each simulation) was a crucial factor. In order to perform the test as efficiently as possible we constructed a three-dimensional subsidiary grid $P(i,j,k)$ containing the information of which particle (if any) is adsorbed within a given discrete space element (a cubical box having a size comparable to the spheroid minor semiaxis b). Then, the overlapping test was performed more efficiently by searching within the ''boxes'' for particles adsorbed in the vicinity of the virtual particle position.

Adsorption kinetics was simulated using the above calculation scheme by introducing the dimensionless adsorption time defined as

$$\tau = \frac{N_{\mathrm{att}}}{N_{\mathrm{ch}}} = \frac{N_{\mathrm{att}}}{(1/S_g)}, \tag{22}$$

where N_{att} is the overall number of attempts at placing the virtual particle and $N_{\mathrm{ch}}=1/S_g$ is the characteristic number of particles.

Some characteristic results obtained for prolate spheroids and relatively short adsorption times ($\tau<5$) are presented in Fig. 5. Both the 2D and 3D kinetic runs obtained for $A=0.2$ are plotted together with the analytical results stemming from Eqs. (19) and (20). It can be observed that the analytical solutions describe well the exact data for $\tau<2$. In contrast, the Langmuir model, giving the kinetic expression Eq. (21) poorly describes the numerical simulations. It can easily be noticed from the kinetic data shown in Fig. 5 that the amount of particles adsorbed after a given time under the 3D regime is almost four times larger than for the flat adsorption. This effect seems to have considerable implications for protein adsorption kinetics.

In Fig. 6 the influence of the parameter A on adsorption kinetics of oblate spheroids is plotted including the case of spheres when $A=1$. It can again be observed that the analytical expressions [Eqs. (19) and (20)] describe well the adsorption runs for short times. Also, the decrease in A (more flattened particles) increased the number of adsorbed particles.

It should also be noted that the saturation of the kinetic curves shown in Figs. 5 and 6 is only apparent due to a considerable decrease in particle adsorption rate for higher surface concentrations. This is the reason why in adsorption studies involving bioparticles (e.g., proteins[10]) and colloids[11,12] these apparent kinetic saturations were interpreted as an indication of true thermodynamic equilibria. This was probably caused by the limiting time of performing adsorption experiments (the dimensionless adsorption time τ usually reached values of the order of 10 in these experiments). If seems that for much longer adsorption times the ''equilibrium'' concentrations would increase to higher values. However, performing precise long-lasting adsorption runs is difficult experimentally.

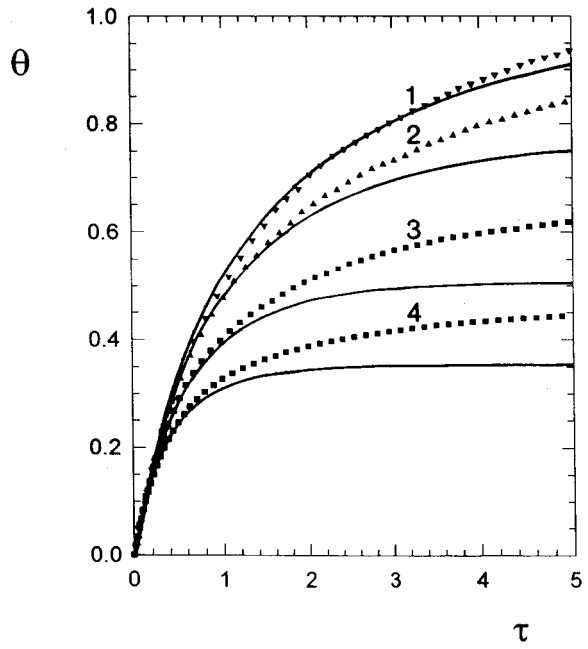

FIG. 6. Kinetics of oblate spheroid adsorption. The dependence of the dimensionless concentration $\theta=\pi a^2 N$ on the dimensionless adsorption time τ determined numerically (points) for various A: (1) $A=0.1$; (2) $A=0.2$; (3) $A=0.5$; (4) $A=1$ (spheres). The continuous lines show the analytical results calculated from Eqs. (19) and (20).

A further considerable increase of the surface concentration can be demonstrated theoretically by plotting the MC-RSA kinetic simulations in an appropriate coordinate system compressing the infinite τ domain into a finite one. As discussed previously[23,27] in RSA processes for long adsorption times ($\tau \gg 1$) asymptotic regimes are started due to the presence of isolated targets only (a swiss cheese model). Moreover, these targets (capable accommodating only one particle) are selective, i.e., they can be filled by adsorbing particles of a given orientation only. As a consequence the asymptotic adsorption kinetics is described by a power-law dependence with the exponent inversely proportional to the number of degrees of freedom m

$$\theta_\infty - \theta \sim \tau^{-1/m}, \tag{23}$$

where θ_∞ is the jamming concentration to be determined.

A differentiation of Eq. (23) gives the following expression for the ASF:

$$\phi \sim (\theta_\infty - \theta)^{m+1}. \tag{24}$$

The validity of this conjuncture was confirmed by Widom[18] for the one-dimensional case $m=1$ (adsorption on the line) when $\theta_\infty=0.748$, by Hinrichsen *et al.*[13] and others[14,15] for the two-dimensional case $m=2$ (adsorption of spherical particles on a planar interface when $\theta_\infty=0.547$), for the flat adsorption of anisotropic particles ($m=3$) such as squares,[23] rectangles,[24] spheroids, and spherocylinders,[25–27] when $m=3$, and θ_∞ was found to vary between 0.518 and 0.56 depending on the A parameter.

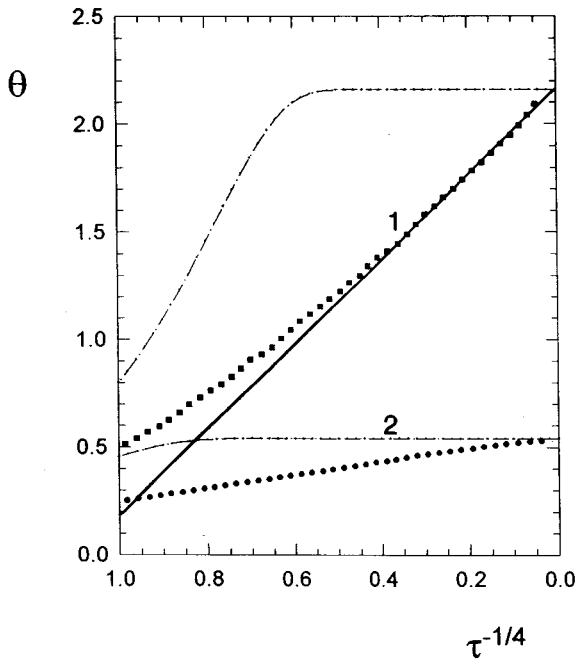

FIG. 7. Adsorption kinetics for longer times (MC-RSA simulations for prolate spheroids, $A=0.2$) expressed as the $\theta=\pi abN$ vs $\tau^{-1/4}$ dependence: (1) 3D adsorption; (2) 2D adsorption. The continuous line denotes the linear fit calculated from Eq. (23) and the -·- lines show the results stemming from the Langmuir model.

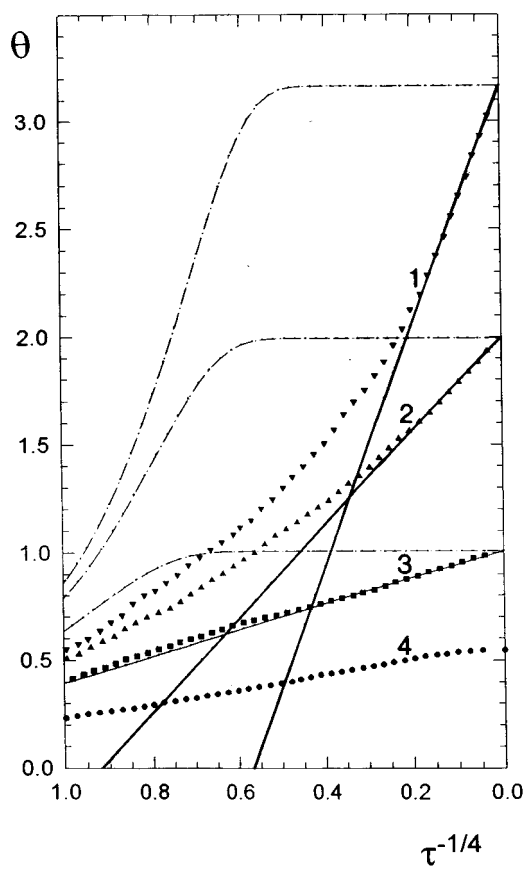

FIG. 8. Adsorption kinetics for longer times (MC-RSA simulations for oblate spheroids) expressed as the $\theta=\pi a^2N$ vs $\tau^{-1/4}$ dependence: (1) $A=0.1$; (2) $A=0.2$; (3) $A=0.5$; (4) $A=0$ (spheres). The continuous line denotes the linear fit calculated from Eq. (23) and the -·- lines show the results stemming from the Langmuir model.

In our case of the 3D adsorption of spheroids one can define four independent degrees of freedom, i.e., the two orientation angles α, β and two spatial coordinates x,y (the z coordinate is determined by the angle β as previously stated). This suggests that the simulation results for long adsorption times should be described by a straight line dependence when plotting θ vs $\tau^{-1/4}$. The results in Figs. 7 and 8 seem to confirm this prediction for both prolate and oblate spheroids. In contrast, the Langmuir model which predicts an exponential approach of the θ_∞ values deviates completely from the exact numerical simulations for $\tau \gg 1$.

It can be deduced, however, that the time of the beginning of the asymptotic adsorption regime increases significantly with a decrease of the A parameter (i.e., for vary elongated or flattened particles).

The existence of the linear regimes (approximated by the solid lines in Figs. 7 and 8) enables one to determine more accurately the θ_∞ values (jamming limit) by extrapolating the θ vs $\tau^{-1/4}$ dependencies generated for long adsorption times. This is advantageous because a direct determination of θ_∞ is not feasible due to the limited value of computer accessible τ values equal to about 10^5 at the most. The monolayers formed by prolate and oblate spheroids after such adsorption times are shown in Figs. 9 and 10, respectively. The precision of the determination of θ_∞ was further increased by taking averages from many computer runs (usually 20–30 for $A<0.2$). In this way a relative accuracy of 1% was attained in most cases.

The θ_∞ values for selected A are collected in Table I (for prolate and oblate spheroids, respectively). Graphically, the dependence of θ_∞ on A for 3D and 2D adsorption of prolate spheroids is shown in Fig. 11. The continuous line presents the fitting function given by

$$\theta_\infty = 0.304 - 0.123A + \frac{0.365}{A} \tag{25}$$

and the broken line denotes the θ_∞ values calculated as an average of a flat orientation and a perpendicular orientation given by

$$\overline{\theta_\infty} = \frac{1}{2}\left[\frac{0.547}{A} + \theta_{\infty 2\mathrm{D}}(A)\right],$$

where $\theta_{\infty 2\mathrm{D}}$ is the jamming concentration for the 2D adsorption of spheroids (also shown in Fig. 11). As can be observed, the numerical value lie well above the averaged value, which suggests that the orientations close to perpendicular are preferred in the adsorption of elongated spheroidal particles (this can also be deduced qualitatively from the monolayer coverages shown in Fig. 10).

Analogous dependency of θ_∞ on A determined numerically for oblate spheroids (with $S_g=\pi a^2$ as previously mentioned) is shown in Fig. 12 together with the fitting function

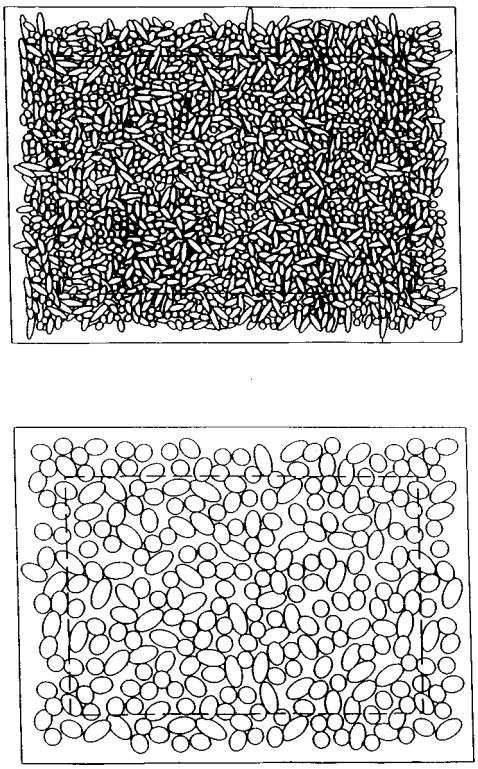

FIG. 9. A top view of ''monolayers'' generated in MC-RSA simulations of 3D adsorption of prolate spheroids ($\tau=10^5$); the upper part for $A=0.2$ ($\theta=2.1$); the lower part for $A=0.5$ ($\theta=0.96$). The broken lines depict the perimeter where the periodic boundary conditions were superimposed.

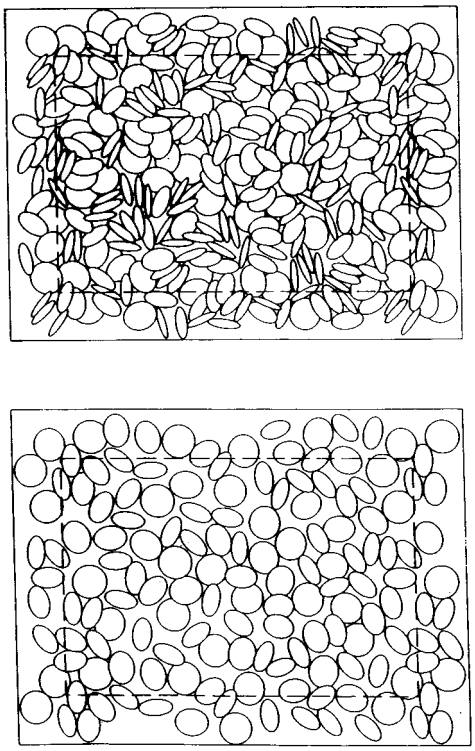

FIG. 10. Same as for Fig. 9 but for oblate spheroids (upper part $A=0.2$, $\theta=1.95$, lower part $A=0.5$, $\theta=0.98$).

$$\theta_\infty = 0.768 - 0.473A + \frac{0.251}{A} \tag{26}$$

and the averaged value

$$\overline{\theta_\infty} = \frac{1}{2}\left(0.547 + \frac{\theta_{\infty 2D}(A)}{A}\right).$$

As can be seen the exact values of θ_∞ exceed the averaged values for the entire range of A.

It should be mentioned, however, that the RSA model exposed in this paper, although useful due to its simplicity, has certain limitations stemming from neglecting the interactions between adsorbing particles and the interface and among particles themselves (this effect should play a role for low coverages). On the other hand, for concentrations close to jamming, the rotary and translational Brownian motion should play a significant role in increasing the probability of particle adsorption.

Adsorption kinetics in which particle diffusion effects are considered can only be performed in terms of very tedious Brownian dynamic simulations to be presented in our future papers.

However, despite its limitation, the RSA model proved adequate for describing adsorption kinetics in the case of spherical colloid particles under a certain combination of flow and diffusion transport conditions.[12,20,21] Using this model it became possible to interpret correctly the kinetic results obtained in various experimental works involving protein, bacteria, and colloids.[12]

The success of the RSA approach in the case of spherical particles would suggest that the theoretical results presented in this work should also prove useful for nonspherical particles. A direct quantitative verification of this hypothesis is planned in our future experiments.

TABLE I. Saturation coverages θ_∞ for prolate and oblate spheroids.

A	Prolate θ_∞	Oblate θ_∞
0.5	0.953±0.003	1.01±0.003
0.333	1.38±0.008	1.38±0.008
0.25	1.78±0.01	1.71±0.007
0.2	2.17±0.01	2.02±0.013
0.1	3.86±0.022	3.19±0.021

IV. CONCLUSIONS

The theoretical analysis based on the RSA model showed that the ASF for the adsorption of spheroidal particles in 3D can well be approximated in the limit of low and moderate surface concentrations by the analytical expression

$$\overline{\phi}(\theta) = 1 - C_1\theta + C_2\theta^2 + 0(\theta^3)$$

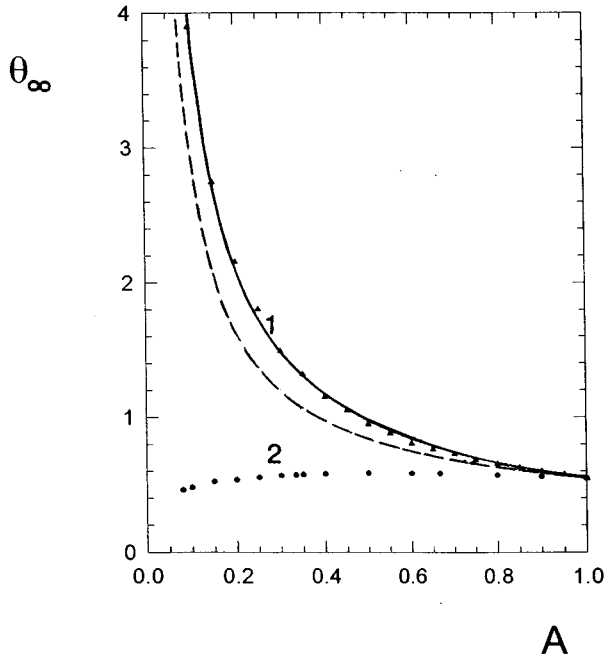

FIG. 11. The dependence of the jamming surface concentration $\theta_\infty = \pi abN_\infty$ on the A parameter determined in MC-RSA simulations for prolate spheroids: (1) 3D adsorption; (2) 2D adsorption. The continuous line shows the results calculated from the fitting function given by Eq. (25) and the broken line denotes the jamming concentration calculated as an average of the side-on and the perpendicular orientation.

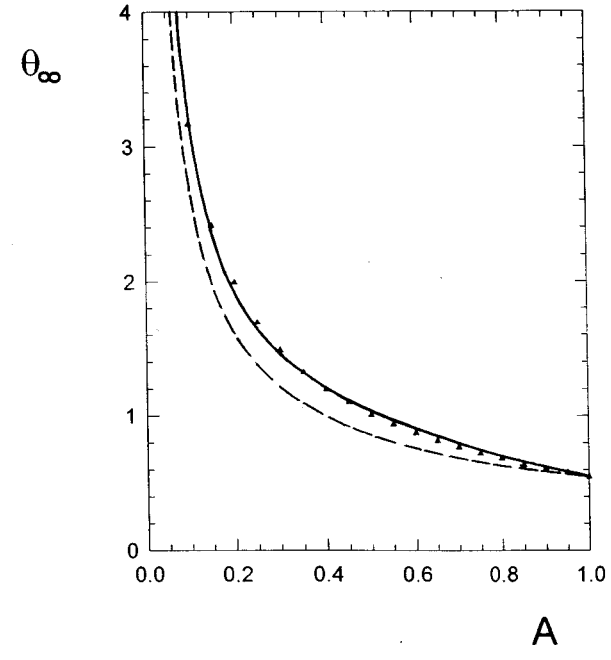

FIG. 12. The dependence of the jamming concentration $\theta_\infty = \pi a^2 N_\infty$ on A for oblate spheroids (3D adsorption). The continuous line shows the results calculated from the interpolating function given by Eq. (26) and the broken line denotes the jamming concentration calculated as an average of the side-on and the perpendicular orientation.

with the constants $C_1 - C_2$ determined numerically and interpolated by the functions given by Eqs. (13)–(18). An integration of this equation produces the analytical kinetic dependencies given by Eqs. (19) and (20).

The exact numerical simulations performed according to the MC-RSA algorithm confirmed the validity of the above analytical expressions for predicting particle adsorption kinetics for low and moderate concentrations.

On the other hand, it was demonstrated that for long times, adsorption kinetics of spheroidal particles can well be expressed by the asymptotic expression

$$\theta_\infty - \theta \sim \tau^{-1/4},$$

which implies that in this limit the ASF becomes

$$\overline{\phi}(\theta) \sim (\theta_\infty - \theta)^5,$$

where the jamming concentrations θ_∞ were found to be considerably larger than for the previously studied case of the 2D (side-on) adsorption.

The analytical results and the extensive numerical simulations of adsorption kinetics suggest that the Langmuir model requiring an empirical knowledge of the maximum concentration θ_∞ is not appropriate for describing localized adsorption of spheroidal particles.

ACKNOWLEDGMENTS

This work was partially supported by KBN Grants Nos. 2P303 039 05 and 7T08B 024 08.

[1] P. Doherety and G. B. Benedek, J. Chem. Phys. **61**, 5426 (1974).
[2] E. Fowler and H. P. Erickson, J. Mol. Biol. **134**, 241 (1979).
[3] P. Schaaf, Ph. Dejardin, and A. Schmitt, Langmuir **3**, 1128 (1988).
[4] P. Schaff and Ph. Dejardin, Colloid Surf. **31**, 89 (1988).
[5] Z. Xia, L. Woo and T. G. M. van de Ven, Biorheology **26**, 359 (1989).
[6] T. Sugimoto, Adv. Colloid Interface Sci. **28**, 65 (1987).
[7] J. J. Peters and G. Dezelic, J. Colloid Interface Sci. **50**, 296 (1975).
[8] M. Ocana, M. Andres, M. Martinez, C. J. Serna, and E. Matijevic, J. Colloid Interface Sci. **163**, 262 (1994).
[9] C. C. Ho, A. Keller, J. A. Odell, and R. H. Otewill, Colloid Polym. Sci. **271**, 469 (1993).
[10] J. Feder and I. J. Giaever, Colloid Interface Sci. **78**, 144 (1980).
[11] B. Vincent, C. A. Young, and Th. Tadros, J. Chem. Soc. Faraday I **76**, 665 (1980).
[12] Z. Adamczyk, B. Siwek, M. Zembala, and P. Belouschek, Adv. Colloid Interface Sci. **48**, 151 (1994).
[13] E. L. Hinrichsen, J. Feder, and T. Jossang, J. Stat. Phys. **44**, 793 (1986).
[14] P. Schaaf and J. Talbot, J. Chem. Phys. **91**, 4401 (1989).
[15] P. Schaaf and J. Talbot, Phys. Rev. Lett. **62**, 175 (1989).
[16] G. Tarjus, P. Schaaf, and J. Talbot, J. Stat. Phys. **63**, 167 (1991).
[17] J. W. Evans, Rev. Mod. Phys. **65**, 1281 (1993).
[18] B. Widom, J. Chem. Phys. **44**, 3888 (1966).
[19] J. Talbot, P. Schaaf, and G. Tarjus, Mol. Phys. **72**, 1397 (1991).
[20] Z. Adamczyk, M. Zembala, B. Siwek, and P. Warszyński, J. Colloid Interface Sci. **140**, 123 (1990).
[21] Z. Adamczyk, B. Siwek, and M. Zembala, J. Colloid Interface Sci. **151**, 351 (1992).
[22] L. Finegold and J. T. Donell, Nature **278**, 443 (1979).
[23] P. Viot and G. Tarjus, Europhys. Lett. **13**, 295 (1990).
[24] R. D. Vigil and R. M. Ziff, J. Chem. Phys. **91**, 2599 (1989).
[25] J. Talbot, G. Tarjus, and P. Schaaf, Phys. Rev. A **40**, 4808 (1989).
[26] P. Viot, G. Tarjus, S. M. Ricci, and J. Talbot, J. Chem. Phys. **97**, 5212 (1992).
[27] S. M. Ricci, J. Talbot, G. Tarjus, and P. Viot, J. Chem. Phys. **97**, 5219 (1992).
[28] Z. Adamczyk and P. Weroński, Bull Pol. Ac. Chem. **42**, 543 (1994).

[29] Z. Adamczyk and P. Weroński, Langmuir **11**, 4410 (1995).
[30] Z. Adamczyk and P. Weroński, Bull Pol. Ac. Chem. (in press).
[31] J. Talbot, D. Kivelson, M. P. Allen, G. T. Evans, and D. Frenkel, J. Chem. Phys. **92**, 3048 (1990).
[32] G. Tarjus, P. Viot, S. M. Ricci, and J. Talbot, Mol. Phys. **73**, 773 (1991).
[33] T. Boublik, Mol. Phys. **29**, 421 (1975).
[34] W. H. Press, S. A. Teukolsky, W. T. Vetterling, and B. P. Flannery, *Numerical Recipes in Fortran*, 2nd ed. (Cambridge University Press, Cambridge, 1992), p. 295.
[35] J. Vieillard-Baron, J. Chem. Phys. **56**, 4729 (1972).